SCHOTTKY NOISE AND BEAM TRANSFER FUNCTION DIAGNOSTICS

D. Boussard
CERN, Geneva, Switzerland

ABSTRACT
Following the analysis of Schottky signals for the unbunched and the bunched beam cases, a general study of electromagnetic detectors is presented. Here the image-current approach and the Lorentz reciprocity theorem will be used to evaluate the detector (or pick-up) performance for several typical examples. Then, signal-processing techniques, which play an important role in the Schottky signal analysis, will be reviewed. The beam transfer function which relates the beam response to an external excitation also provides very useful information about the accelerator behaviour. It requires an element to excite the beam (kicker) which will be shown to be equivalent to a detector working in reverse. With beam-transfer-function measurements an assessment of beam stability limits can be made, leading to the determination of the overall ring impedance.

The noise generated in an old fashioned electron tube is governed by the Schottky formula which simply reflects the fact that the anode current is composed of individual electrons randomly emitted by the cathode. Very similarly, the beam current in a circular particle accelerator, also exhibits a random component, called the Schottky noise, which results from the large, but finite, number of particles in the beam. In the absence of random quantum emissions (i.e. for hadron machines) the analysis of Schottky noise signals (or Schottky signals, for brevity) is a very powerful tool to study the accelerator behaviour . Historically, Schottky signals have been observed first on unbunched beam machines (CERN ISR),[1,2] leading to the development of the very successful stochastic cooling technique. For bunched beams, the presence of strong "macroscopic" beam signals renders the observation of the tiny Schottky signals more difficult. However improved signal processing techniques have recently made their observation possible.

Following the analysis of Schottky signals for the unbunched and the bunched beam cases, a general study of electromagnetic detectors is presented. Here the image-current approach and the Lorentz reciprocity theorem will be used to evaluate the detector (or pick-up) performance for several typical examples. Then, signal-processing techniques, which play an important role in the Schottky signal analysis, will be reviewed.

The beam transfer function which relates the beam response to an external excitation also provides very useful information about the accelerator behaviour. It requires an element to excite the beam (kicker) which will be shown to be equivalent to a detector working in reverse. With beam-transfer-function measurements an assessment of beam stability limits can be made, leading to the determination of the overall ring impedance.

1 SCHOTTKY SIGNALS

1.1 Unbunched beam, longitudinal

For a single particle circulating in the machine (charge e, revolution period $T_i = 1/f_i$), the beam current, at a given location in the ring, is composed of an infinite train of delta pulses (Fig. 1a) separated in time by T_i. In frequency domain, this periodic waveform is represented by a line spectrum (Fig. 1b), the distance between lines being $f_i = \omega_i/2_\pi$.

$$i_i(t) = ef_i \sum_{n=-\infty}^{+\infty} \exp jn\omega_i t \quad . \tag{1}$$

Looking at positive frequencies only:

$$i_i(t) = ef_i + 2ef_i \sum_{n=1}^{\infty} \cos n\omega_i t \quad . \tag{2}$$

The first term represents the DC component, the others are simply the successive harmonics of the revolution frequency.

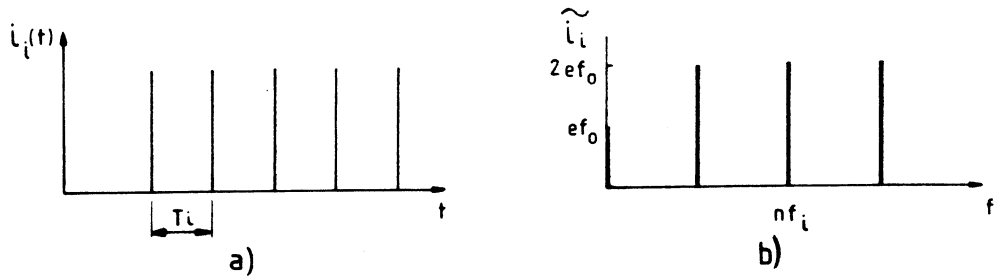

Fig. 1 a) Time domain δ pulses b) Frequency domain: line spectrum

For N particles, randomly distributed in azimuth along the ring circumference (debunched beam case) and having slightly different ω_i, each line at frequency nf_i which is infinitely narrow in the case of a single particle, will be replaced by a band of frequencies (Schottky band) whose width is simply:

$$\Delta f = n\,\Delta f_i = n\, f_o\, \eta\, \frac{\Delta p}{p} \quad , \tag{3}$$

Δf_i is the spread in particle's revolution frequencies resulting from the relative momentum spread $\Delta p/p$ and the machine parameter $\eta = (1/\gamma_t^2 - 1/\gamma^2)$. f_o is the average revolution frequency.

When averaging equation (2) over N particles, only the DC terms remain ($i_{DC} = Nef_o$), the other components cancel due to the random azimuth phase factor. However, the r.m.s. current per band which is given by the sum:

$$\langle i^2 \rangle = [2ef_o (\cos \theta_1 + \cos \theta_2 + \ldots + \cos \theta_i + \ldots + \cos \theta_N)]^2 \qquad (4)$$

does not vanish because of the $\cos \theta^2$ terms. One obtains:

$$i_{rms} = \sqrt{\langle i^2 \rangle} = 2ef_o \sqrt{N \langle \cos \theta_i \rangle^2} \qquad (5)$$

$$\boxed{i_{rms} = 2ef_o \sqrt{\frac{N}{2}}} \quad . \qquad (6)$$

The r.m.s. current per band (Schottky current) is independent of n (harmonic number) and proportional to the square root of the number of particles N.

As indicated on Fig. 2, the power spectral density, proportional to $\langle i^2 \rangle / \Delta f$, decreases with n until overlap occurs ($\Delta f > f_o$). For a given band the local power density is obviously proportional to the number of particles per unit frequency. If the parameter η is known (η may be frequency dependent), the measurement of the power spectral density, in one particular Schottky band gives directly the $\Delta p/p$ distribution of the beam.

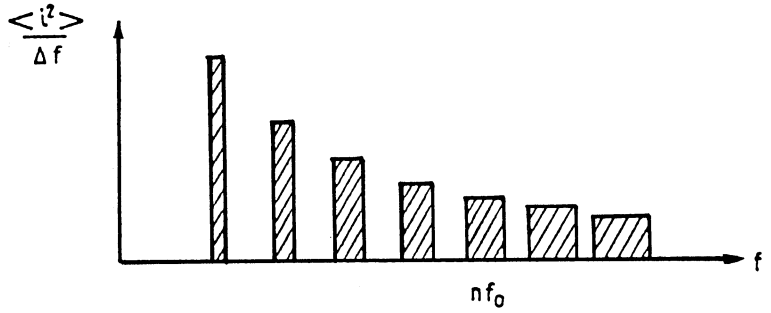

Fig. 2 Power spectral density of Schottky lines with increasing n.

This forms the basis of $\Delta p/p$ beam distribution measurements in DC coasting machines, (cooling and accumulation rings in particular).

Note that the noise signals pertaining to successive Schottky bands are not correlated because the random azimuthal phase factor is multiplied by n in Eq. (4).

1.2 Unbunched beam, transverse

For a single particle, the beam current $i_i(t)$ must be replaced by the dipole moment: $d_i(t) = a_i(t) . i_i(t)$, where $a_i(t)$ is the transverse displacement. The i^{th} particle executes a sinusoidal betatron oscillation, of amplitude a_i, which can be written:

$$a_i(t) = a_i \cos (q_i \omega_i t + \varphi_i) \tag{7}$$

Here $q_i f_i$ is the observed frequency, at a fixed location in the ring, q_i being the non integer part of the betatron tune (Fig. 3a)

In frequency domain:

$$d_i(t) = a_i \cos(q_i \omega_i t + \varphi_i) \; ef_o \sum_{n=-\infty}^{+\infty} \exp jn\omega_i t \tag{8}$$

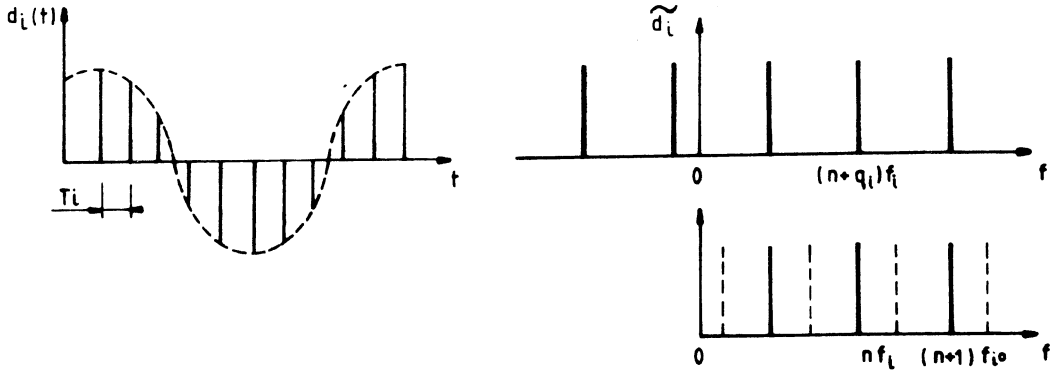

(a) (b)

Fig. 3 Time (a) and Frequency (b) domain representations of a single-particle transverse oscillation

$$d_i(t) = a_i \; ef_o \; R_e \left\{ \sum_{n=-\infty}^{+\infty} \exp j[(n + q_i) \; \omega_i t + \varphi_i)] \right\} . \tag{9}$$

The spectrum is again a series of lines spaced by the revolution frequency of the i^{th} particle, but shifted in freqency by $q_i f_i$. Looking at positive frequencies only (Fig. 3b) one obtains two betatron lines per revolution frequency band as in the case of an amplitude-modulated carrier which exhibits two symmetrical sidebands.

For N particles in the beam, again randomly distributed in azimuth and in betatron phases, averaging equation (9), for a given value of n + q, gives:

$$\langle d \rangle = 0 \quad ; \quad \langle d^2 \rangle = \langle a_i^2 \rangle \; e^2 \; f_o^2 \; \frac{N}{2} \tag{10}$$

$$d_{rms} = ef_o \; a_{rms} \sqrt{\frac{N}{2}} \; . \tag{11}$$

Again, the total power per Schottky band is independent of its location in the frequency spectrum; it is proportional to the number of particles in the beam and to the square of the r.m.s. oscillation amplitude.

Each Schottky band has now a finite width which results from the spread of revolution frequencies $\Delta f_i/f_o = \eta\, \Delta p/p$ and from the spread of betatron frequencies Δq_i. The latter usually comes from the machine chromaticity ξ: $\Delta q_i = Q\xi \Delta p/p$, but may also result from space charge, beam-beam or nonlinear effects.

The line width of two adjacent Schottky bands $(n \pm q)$ is given by:

$$\Delta f = (n \pm q)\, \Delta f_i \pm 2\pi f_o\, \Delta q_i \tag{12}$$

$$\Delta f = f_o \frac{\Delta p}{p} \left[(n \pm q)\, \eta \pm Q\xi \right] \tag{13}$$

if only chromaticity contributes to the betatron frequency spread.

Equation (13) shows that the width of the two Schottky bands is not the same, due to the machine chromaticity. However, by comparing the two bands $n \pm q$, one can determine the Δq_i of the beam. Even more, if one can identify similar points on the distribution (resonances, for instance), their q can be determined by the formula:

$$q = \frac{1}{2}\left(1 + \frac{\Delta f_c}{f_o}\right) \tag{14}$$

Δf_c being the measured frequency difference between them. This technique was extensively used in the ISR to monitor the working line of the machine distribution in transverse tunes.

Comparing equations (10) and (6) gives a direct measure of the r.m.s. betatron amplitude:

$$\frac{d_{rms}}{i_{rms}} = \frac{a_{rms}}{2} \quad . \tag{15}$$

Equation (15) can be used to measure directly the transverse beam emittance, if the beam distribution is known. This obviously requires well calibrated longitudinal and transverse detectors to measure accurately d_{rms} and i_{rms} unless only relative measurements are sought (evolution of AA transverse emittance, for instance).

1.3 Bunched beam, longitudinal

In the bunched beam case, every individual particle executes synchrotron oscillations at the frequency $\Omega_s/2\pi$. The time of passage of the particle in front of the detector is modulated according to:

$$\tau_i(t) = \hat{\tau}_i \sin (\Omega_s t + \psi_i) \tag{16}$$

$\tau_i(t)$ is the time difference with respect to the synchronous particle (frequency f_o) and $\hat{\tau}_i$ is the amplitude of the synchrotron oscillation, assumed to be linear. In time domain, the beam current is represented in Fig. 4, as a series of delta pulses, with a modulated time of passage. It can be written:

$$i_i(t) = ef_o + 2ef_o R_e \left\{ \sum_{n=1}^{\infty} \exp jn\omega_o(t + \hat{\tau}_i \sin (\Omega_s t + \psi_i)) \right\} . \tag{17}$$

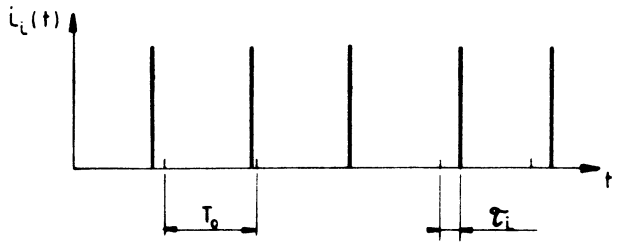

Fig. 4 Time domain representation of a single particle current in a bunched beam.

Using the relation:

$$\exp (j (z \sin \theta)) = \sum_{p=-\infty}^{+\infty} J_p(z)\, e^{jp\theta} \tag{18}$$

where J_p is the Bessel function of order p, one can expand the nth harmonic in equation (17) and obtain:

$$i_n = 2ef_o R_e \left\{ \sum_{p=-\infty}^{+\infty} J_p(n\omega_o \hat{\tau}_i) \exp j(n\omega_o t + p\Omega_s t + p\psi_i) \right\} . \tag{19}$$

Each revolution frequency line (nf_o) now splits into an infinity of synchrotron satellites, spaced by $\Omega_s/2\pi$, the amplitudes of which being proportional to the Bessel functions of argument $n\omega_o\hat{\tau}_i$ as shown in Fig. 5.

The amplitudes of the synchrotron satellites become negligible beyond a certain value of p. This is because $J_p(x) \simeq 0$ for $p > x$ if x is large. Therefore, the synchrotron satellites are, in practice, confined into a limited bandwidth:

$$2p\Omega_s = 2n\omega_o \hat{\tau}_i \Omega_s . \tag{20}$$

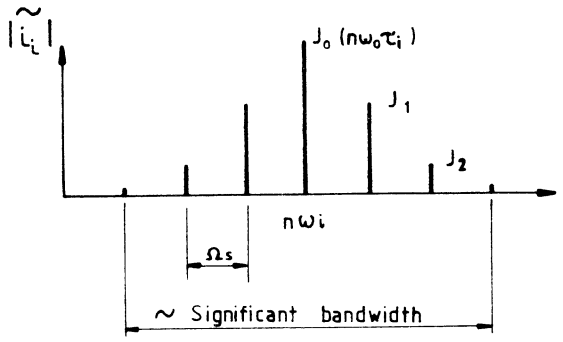

Fig. 5 Decomposition of each revolution line into synchrotron satellites

The spread in the instantaneous revolution frequency of the i^{th} particle due to the synchrotron oscillation is simply:

$$2\Delta\omega_i = 2\Omega_s\, n\omega_o \hat{\tau}_i \quad . \tag{21}$$

Consequently, for large values of n, the significant bandwidth around line n is the same as that of a beam of many particles having the same $\Delta\omega_i$ and therefore the same $\Delta p/p$.

Consider now the case of many particles, with randomly distributed synchrotron phases ψ_i and $\hat{\tau}_i$ ranging from 0 to $\hat{\tau}_m$ ($2\hat{\tau}_m$ being the total bunch length).

For a given n, the central line (p = 0) shows the same phase factor (exp $jn\omega_o t$) for all particles: the current in the central line is therefore proportional to N and not $\sqrt{N}$; this is simply the macroscopic RF current of the bunch. On the contrary, the synchrotron satellites ($p\neq 0$) add r.m.s. wise because of the random phase factor exp $j(n\omega_o t + p\Omega_s + p\psi_i)$ (Fig. 6).

Each line is infinitely narrow if the synchrotron oscillation is purely linear (Ω_s is the same for all particles) and if the machine has no imperfections. However, magnet and RF fluctuations broaden in practice each individual line. In addition a spread in synchrotron frequency within the bunch $\Delta\Omega_s$ transforms each satellite ($p\neq 0$) into a band of width $p\Delta\Omega_s$. For large values of n, overlap between successive synchrotron satellites ($p\Delta\Omega_s > \Omega_s$) can occur within the significant width of the Schottky band of order n. (Fig. 6b)

If we consider two Schottky bands with different values of n, their corresponding synchrotron satellites (of order p) are correlated. This results from Eq. (19), where the random phase factor $p\psi_i$ is the same, even for different values of n.

Another way to look at the coherence between successive Schottky bands is to examine the bunch signal in time domain (Fig. 7). It is composed of a steady component

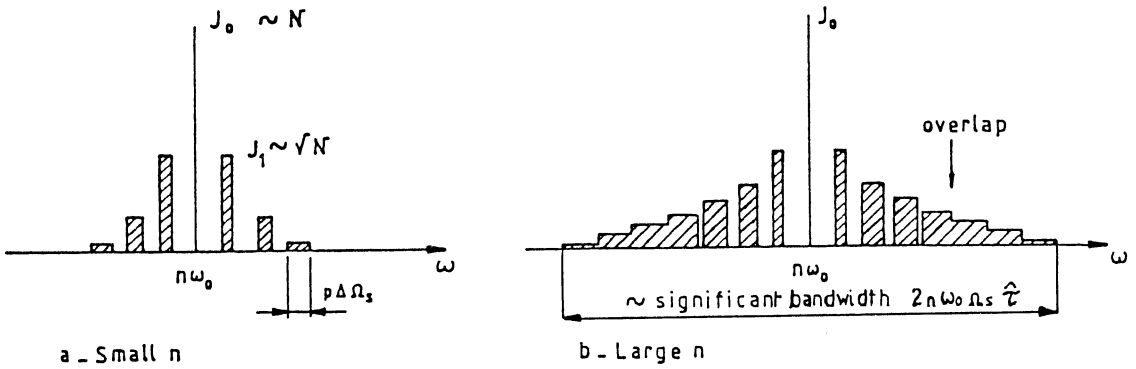

Fig. 6 Longitudinal Schottky spectrum of a bunched beam.

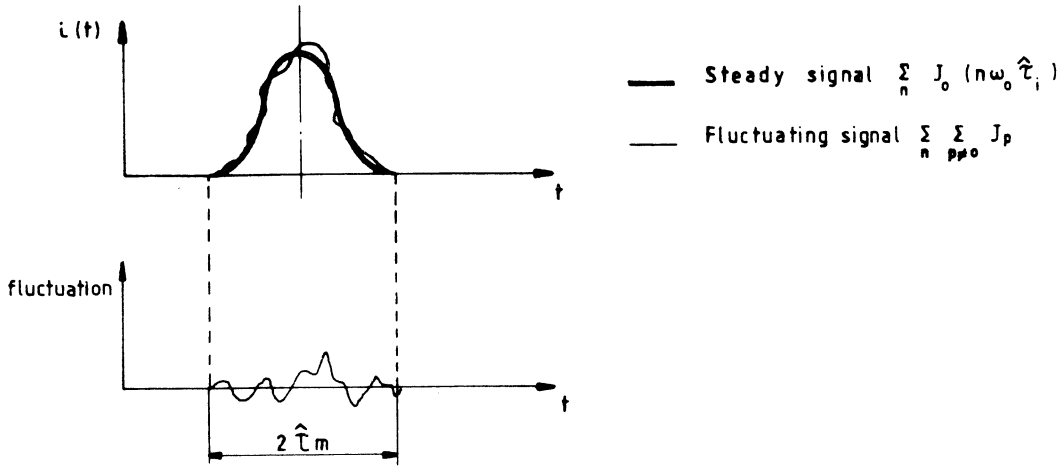

Fig. 7 Time domain of representation of bunched beam Schottky signal.

(macroscopic signal resulting from the terms: $\sum_n J_0 (n\omega_0 \hat{\tau}_i)$) and a fluctuating Schottky signal ($\sum_n \sum_{p\neq 0} J_p (n\omega_0 \hat{\tau}_i)$). The fluctuating signal extends in time over $2\hat{\tau}_m$, and can be Fourier decomposed into components at multiples of the fundamental bunch frequency $f_b = 1/2\hat{\tau}_m$. All information concerning the Schottky signal is contained into those components (in the limit $\Omega_s << \omega_0$). In other words significant information about the Schottky signal only appears every f_b frequency interval, the other spectral lines in (19) (every f_0) simply give redundant information, i.e., they are correlated.

As a consequence, sampling of Schottky signals at f_0, which folds many nf_0 bands on top of each other and only gives one Schottky signal, does not introduce any loss of information, if the bandwidth before sampling is limited to $\pm f_b/2$.

1.4 Bunched beam, transverse

Here we have to combine the amplitude modulation (betatron oscillation) and the time modulation (synchrotron oscillation). One obtains:

$$d_i(t) = a_i \cos(q_i\omega_o t + \varphi_i)\ ef_o\ R_e\left\{\sum_{n=-\infty}^{+\infty} \exp\ jn\omega_o(t + \hat{\tau}_i \sin(\Omega_s t+\psi_i))\right\} \quad . \tag{22}$$

If q_i is independent of ω_i, the n^{th} sum becomes:

$$d_n = ef_o a_i\ R_e\left\{\sum_{p=-\infty}^{+\infty} J_p((n\pm q)\omega_o\hat{\tau}_i)\ \exp\ j[((n\pm q)\omega_o+p\Omega_s)t+p\psi_i+\varphi_i]\right\} \quad . \tag{23}$$

Again, each betatron line splits into an infinite number of synchrotron satellites (Fig. 8). The significant bandwidth, as in the longitudinal case, approaches that of coasting beams with the same $\Delta p/p$, for large values of n. On the contrary, for small values of n, most of the energy is concentrated in the p = 0 line.

Fig. 8 Decomposition of each betatron line into synchrotron satellites.

For a non-zero chromaticity, the argument of the Bessel function $(n \pm q)\omega_o\hat{\tau}_i$ should be replaced by $[(n \pm q) - Q\xi/\eta]\ \omega_o\hat{\tau}_i$. In this case, the relative amplitudes of the synchrotron satellites also depend on the chromaticity. In particular, for the chromatic frequency:

$$\omega_\xi = Q\,\frac{\xi}{\eta}\,\omega_o \tag{24}$$

only the term J_o is significant: all the energy of the nth Schottky band is concentrated in the central line.

With many particles, we should average over the two random variables φ_i and ψ_i. Unlike the longitudinal case, the central lines (p=0) add up r.m.s. wise due to the random betatron phase factor φ_i , the consequence being that there is no transverse macroscopic signal. Successive bands are correlated as in the longitudinal case, again, because all the signal is concentrated in the time interval $2\hat{\tau}_m$ and not $T_o = 1/f_o$ as if the beam were unbunched.

The width of the central line is determined by RF and magnetic field fluctuations, but also by transverse nonlinearities (tune spread due to octupole fields, beam-beam or

space charge forces). In addition, the synchrotron satellites are broadened by the spread in synchrotron frequencies within the bunch (width $p\Delta\Omega_s$ as in Fig. 6).

The total power per band (for a given n) is given by:

$$\langle d_n \rangle^2 = e^2 f_o^{\,2} \langle a^2 \rangle \frac{N}{2} \sum_p J_p^{\,2} ((n \pm q)\, \omega_o \hat{\tau}_i) \quad . \tag{25}$$

With the identity:

$$\sum_{p=-\infty}^{+\infty} J_p^{\,2}(x) = 1 \tag{26}$$

one obtains:

$$\langle d_n \rangle^2 = e^2 f_o^{\,2} \langle a^2 \rangle \frac{N}{2} \quad . \tag{27}$$

The total power per band is the same as in the coasting beam case, for the same total number of particles and the same transverse oscillation amplitude (Fig. 9).

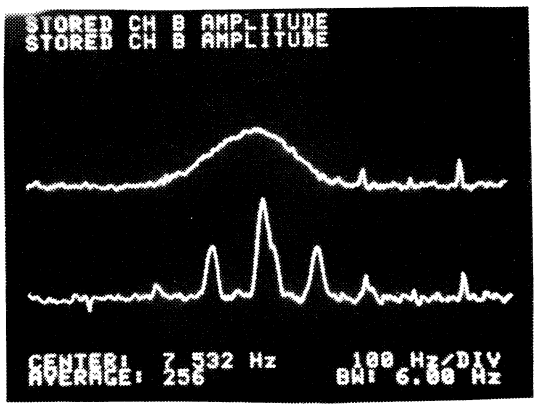

Fig. 9 Horizontal Schottky signals in the SPS.
Top: debunched beam
Bottom: bunched beam.

2 BEAM DETECTORS

2.1 The image-current approach

Consider the very simple geometry of Fig. 10a, where a round beam circulates in the center of a cylindrical smooth vacuum chamber. This is a two-dimensional problem, and it is well known that the electromagnetic fields are purely transverse, as in a coaxial line,

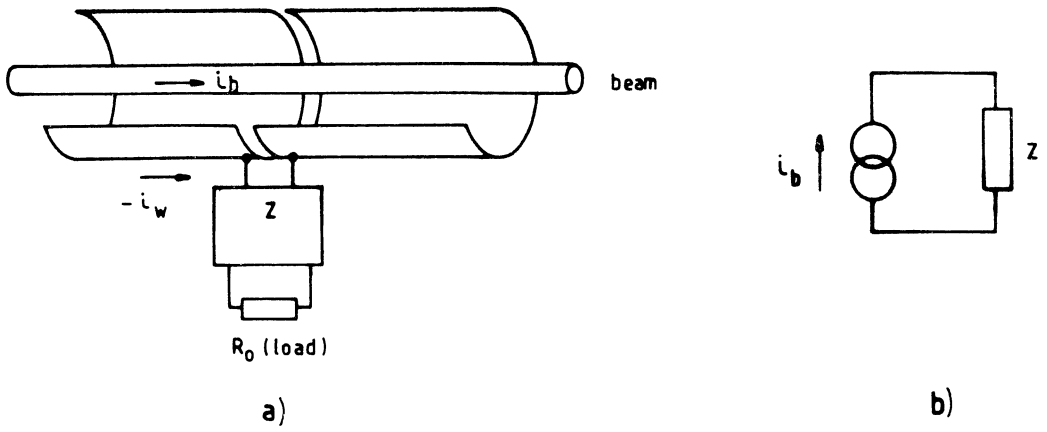

Fig. 10 The beam is equivalent to a current source flowing into the detector impedance.

in the limit $v = c$. It follows that for all frequencies the beam and wall currents are opposite:

$$i_b = -i_w \tag{28}$$

Equation (28) is only valid up to some upper frequency, depending on the particle relativistic factor γ and the transverse dimensions of the vacuum chamber. However, for most practical cases (high energy storage rings) this is not a limitation.

If now we cut a gap in the circular wall we introduce a coupling between the inside and the outside of the vacuum pipe. The latter is characterised by the impedance Z which we can measure between the two sides of the gap. As the energy lost by the beam when passing through the detector is much smaller than the particle's energy, the current i_b, and hence i_w is independent of the gap voltage: it means that the wall current i_w which flows through Z can be represented by a pure current source (Fig. 10b).

The detector, which seen from the gap appears like an impedance Z, delivers its output signal in the load R_o (Fig. 10a). The sensitivity of the detector (longitudinal in this case) is defined by:

$$\boxed{S = \frac{V_{out} \text{ in } R_o}{i_b}} \tag{29}$$

For a lossless network between gap and R_o, one can easily obtain, from power considerations:

$$S = \sqrt{R_o . R_e Z} \quad .$$

The following examples will illustrate the image current approach for the evaluation of beam detectors (or beam pick-ups).

a) The resistive-gap pick-up

In this case the load resistor R_o is simply connected to the vacuum chamber gap. However, to provide a low impedance DC return path for the wall current, a short-circuited coaxial line is built around the vacuum chamber, as shown on Fig. 11. The line is filled with lossy material (ferrites) such that, for the operating frequency of the pick-up, it appears as a terminated line. This introduces a low-pass characteristic in the detector response.

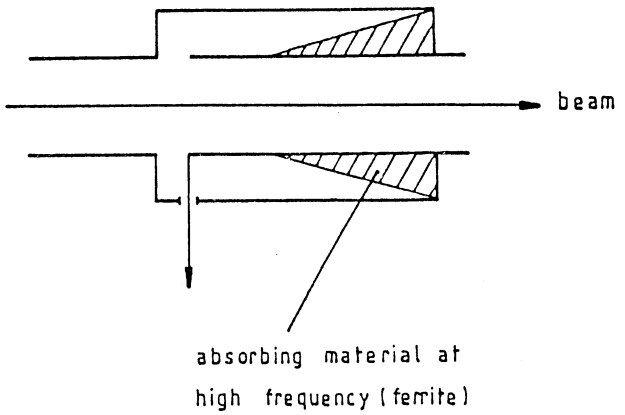

Fig. 11 Resistive-gap pick-up

The upper frequency limit is determined by the parasitic capacitance at the gap. Making R_o small (several parallel resistors) will push the upper frequency limit, at the expense of sensitivity.

The SPS wide-band longitudinal detector[3] uses eight parallel 50 Ω strip lines symmetrically connected to the gap, and a ferrite loaded coaxial line with 25 Ω characteristic impedance. This arrangement gives Z = 5 Ω. The eight gap signals are combined in an eight port power combiner giving an overall sensitivity, in a 50 Ω load:

$$S = 5\sqrt{8} = 14\ \Omega$$

instead of the maximum $S = \sqrt{6.25 \times 50} = 17.6\ \Omega$ if no power would be lost in the ferrites (very high impedance coaxial line).

The bandwidth extends form 4 MHz to 4 GHz with almost no resonances. To improve the low-frequency response the inductance of the short circuited line can be increased by lossless ferrites, but high-frequency resonances may be difficult to suppress.

b) The directional-coupler pick-up

As shown on Fig. 12a, there are two gaps in this detector, joined together by a piece of coaxial line of characteristic impedance R_o, surrounding the vacuum chamber. With the two load resistors R_o which are connected to each gap, one can draw the equivalent

circuit of Fig. 12b. The two beam current sources, at each gap, are in opposite direction, and are shifted in phase by the beam transit time.

The current flowing in the load R_o on the right is the sum of the contributions from the two current sources:

$$\frac{i_b}{2} \exp(-j\omega\ell / v_\varphi) \qquad \text{left source}$$

$$-\frac{i_b}{2} \exp(-j\omega\ell / v_p) \qquad \text{right source}$$

v_φ and v_p being the wave and beam velocities and ℓ the distance between gaps.

The total current:

$$\frac{i_b}{2}\left(\exp\left(-j\frac{\omega\ell}{v_\varphi}\right) - \exp\left(-j\frac{\omega\ell}{v_p}\right)\right) \tag{30}$$

vanishes if v_p and v_φ are equal.

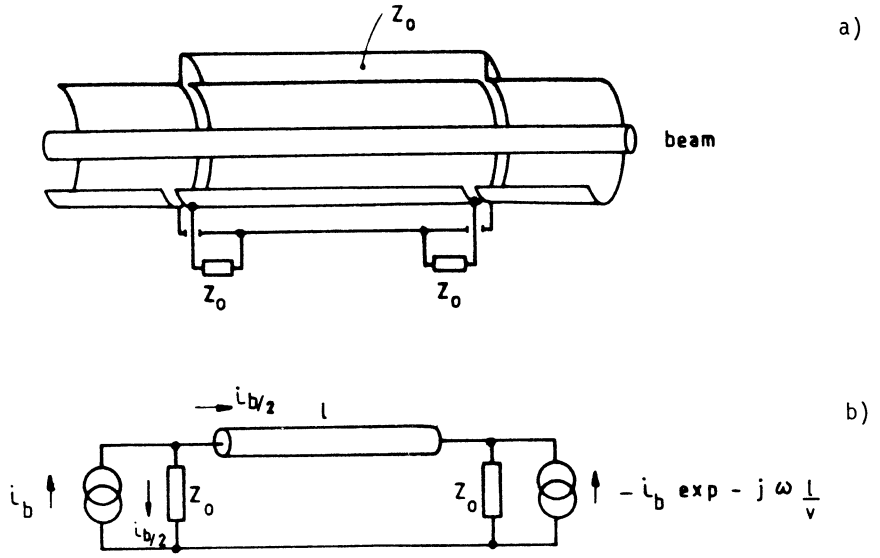

Fig. 12 Directional-coupler pick-up
a): schematics, b): equivalent circuit

For the load R_o on the left, one finds easily the current:

$$\frac{i_b}{2}\left(1 - \exp\left(-j\omega\left(\frac{1}{v_\varphi} + \frac{1}{v_b}\right)\ell\right)\right) \tag{31}$$

and the corresponding sensitivity:

$$S = \frac{R_o}{2} (1 - \exp(-2j\omega \frac{\ell}{v})) \qquad (32)$$

for $v_p = v_\varphi = v$.

If this synchronous condition is fulfilled, for instance if $v_p = c$ and the coaxial line is in vacuum, this detector is directional: the signal only appears at the upstream port (with respect to beam velocity). With counterrotating beams (p and pbars for instance) the directional pick-up can separate the signals from the two types of particles. In practice the directivity is of the order of 30 to 35 dB. Note that directivity can, in principle, be obtained also by combining the signals of several identical detectors.

The sensitivity of the detector, given by Eq. (32) is frequency dependent (Fig. 13). It shows a succession of zeros and maxima corresponding to:

$\ell = \frac{\lambda}{2}, \lambda, \frac{3\lambda}{2}$: zeros

$\ell = \frac{\lambda}{4}, \frac{3\lambda}{4}, \frac{5\lambda}{4}$: maxima

the sensitivity being simply R_o at the maxima.

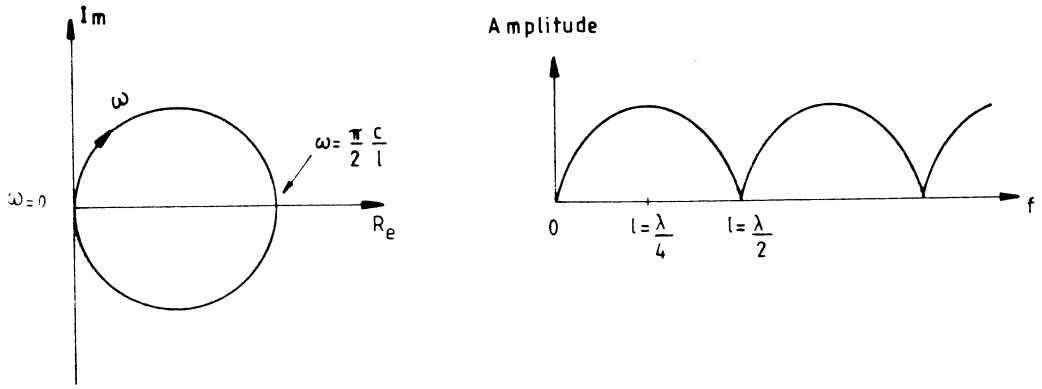

Fig. 13 Transfer functions of the directional-coupler pick-up.

The transient response of the detector can be obtained by making the inverse Fourier transform of Eq. (32), but it is obvious from the equivalent circuit of Fig. 12b that it is composed of two opposite delta pulses separated in time by twice the transit time ($2\ell/c$) (Fig. 14a).

Several identical pick-ups can be combined to increase the overall sensitivity. With power combiners, the output signals are added power wise giving an overall sensitivity $S = R_o\sqrt{n}$ for identical detectors, and the same frequency response. One can also

combine several directional coupler detectors in cascade and obtain, with the proper delays, a transient response as in Fig. 14b. There the maximum sensitivity is proportional to η, but the frequency response now shows a sin f/f curve peaked at $\ell = \lambda/4$. In other words, the higher sensitivity (proportional to η) results in a narrower bandwidth.

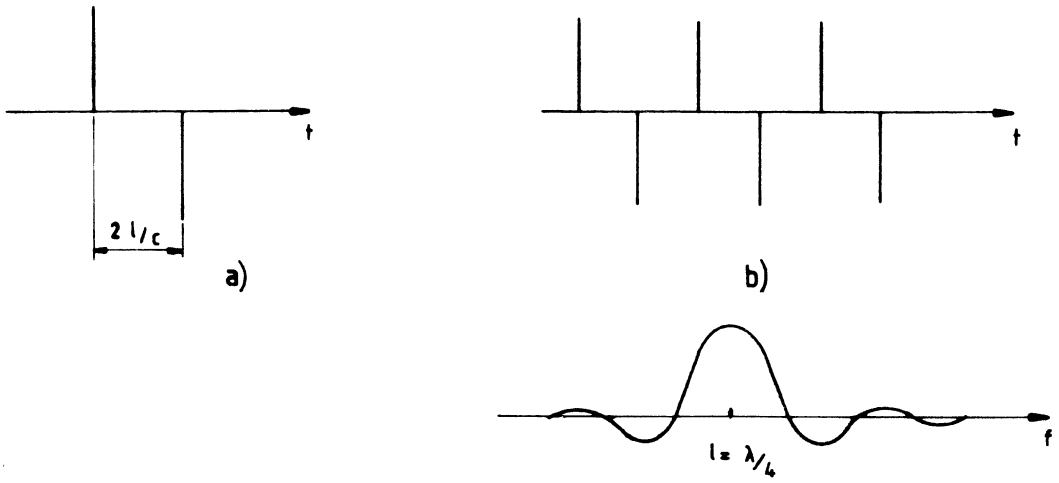

Fig. 14 Transient response of directional coupler
a): single
b): multiple (with the associated frequency response).

Directional coupler pick-ups are in fact mostly used as transverse detectors. With several strips symmetrically arranged in the vacuum chamber, as in Fig. 15a, the total wall current i_w should be replaced by $i_w\ \theta/2\pi$ for each strip, provided the beam is in the center. For a non-centered beam the problem is truly three dimensional near the gaps. By approximating the electromagnetic field by that of a pure TEM wave one can obtain the wall current distribution along the vacuum chamber azimuth which obviously depends on the beam position. For small beam displacement, Δx, the difference of the signals of two opposite strip lines is proportional to Δx:

$$\Delta V = V_2 - V_1 = S_\Delta\ i_b\ \Delta x \tag{33}$$

S_Δ being defined by equation (33) as the transverse sensitivity of the detector (in ohms/meter).

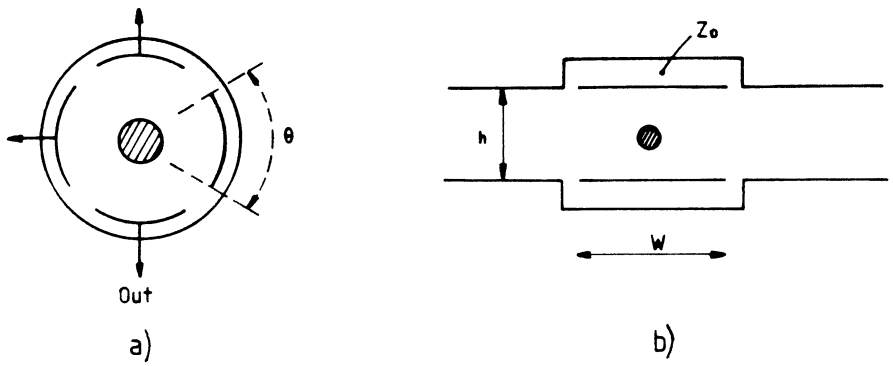

Fig. 15 Cross section of transverse directional-coupler pick-up
a): circular
b): rectangular

In the case of a rectangular geometry, often used in wide-aperture cooling rings for instance, the sensitivity S_Δ is given by:

$$S_\Delta = \frac{R_o}{2h} \left(\tanh \frac{\pi w}{h}\right) \quad . \tag{34}$$

The form factor tanh(πw/h) simply reflects the fact that some fraction of the wall current flows outside the strip line gaps.

This type of pick-up (sometimes called loop coupler) is widely used in cooling systems. It offers a good compromise between bandwidth (of the order of one octave) and sensitivity. The signals of many couplers are often added power wise on a combiner board, inside vacuum, to increase the overall sensitivity. If only one type of particle is present, the downstream resistor R_o, where no current flows, can be replaced by a short circuit (hence the name of loop coupler), but microwave resonances may be harmful in this case.

c) The electrostatic pick-up

If the coaxial line of Fig. 12a is much shorter than the wavelength ($\ell \ll \lambda$), it can be represented by a simple capacitor $C = \ell/R_o v_\varphi$ (Fig. 16a). For a very high load resistor, the equivalent circuit of Fig. 16b represents the electrostatic detector, with the two current sources phase shifted by $\omega\ell/v_b$.

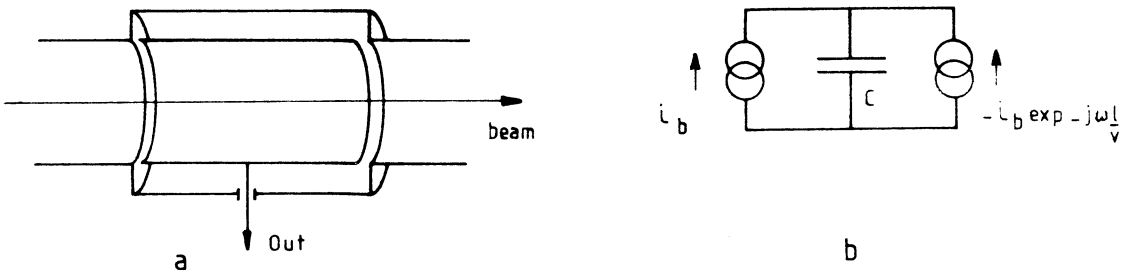

Fig. 16 The electrostatic pick-up

The voltage developed on the line (or the electrode) is simply:

$$V = \frac{1}{jC\omega} \left[i_b - i_b \exp\left(-j\omega\, \ell/v_b\right)\right] \tag{35}$$

$$V \simeq \frac{i_b}{jC\omega} \cdot j\frac{\omega\ell}{v_b} \quad . \tag{36}$$

The quantity $\ell i_b/v_b$ is the beam charge q contained in the detector length, (assuming a slowly varying charge distribution with respect to the electrode length). It follows:

$$V = q/C \tag{37}$$

as the electrostatic theory would have given immediately.

For $v_\varphi = v_b$ and in the approximation of a high load resistor, Eq. (36) combined with $C = \ell/R_o v_\varphi$ leads to the very simple result:

$$S = R_o \quad .$$

The sensitivity is independent of the frequency and of the length of the detector. Of course this is only true at medium frequencies. The non-infinite load resistor (usually an amplifier with high input impedance) introduces a low frequency cut off whereas at high frequencies the approximation $\ell << \lambda$ is no longer valid.

The transverse version of the electrostatic pick-up can be obtained by splitting the electrode cylinder in two halves along a linear cut. (Fig. 17). Electrostatic theory shows that the difference in voltage between the two plates is a linear function of the beam displacement. Many versions of the transverse electrostatic pick-up with various shapes could be found in the literature (circular, rectangular, elliptical)[4]. They are mostly used for closed orbit measurements (sometimes horizontal and vertical pick-ups are combined in a single unit).

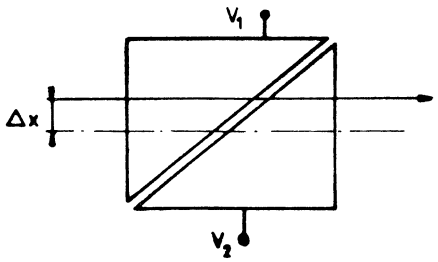

Fig. 17 Transverse electrostatic pick-up linearly cut

If the linearity requirement is less important, the linear cut could be abandoned, for instance in the so called "buttons" to be used in LEP (Fig. 18). There, only the high-frequency response is important, and consequently the load resistor is a 50 Ω cable. The linearity can be restored by a proper algorithm at the signal processing level.

The electrostatic detector can be made resonant, with a coil (or transformer) connected to the electrode. A transverse version is sketched in Fig. 19a, with the equivalent circuit of Fig. 19b.

At resonance the voltage across the plates V' is given by:

$$V' = j\,\omega \frac{\ell}{v_b} R \frac{2\Delta x}{d} i_b \tag{38}$$

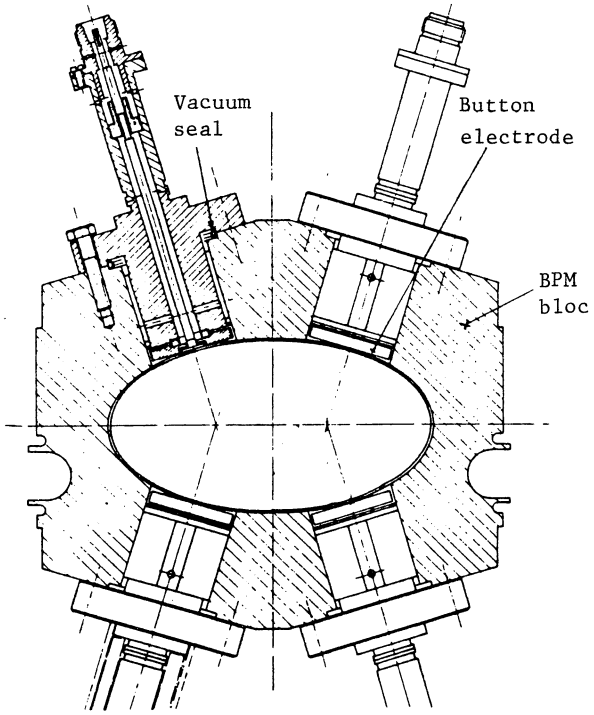

Fig. 18 Cross section of the LEP position detector

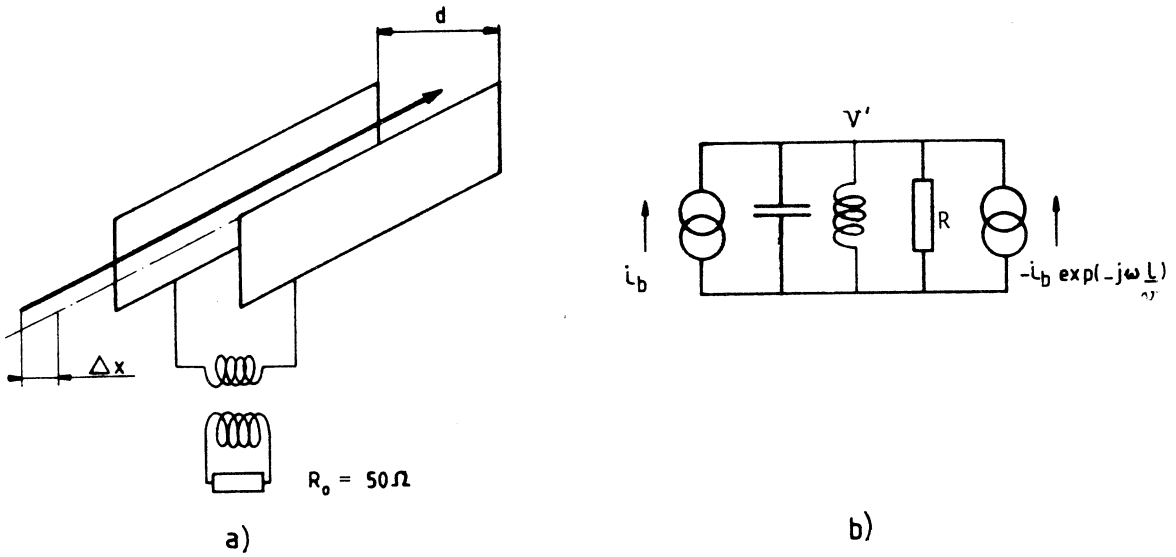

Fig. 19a): Resonant electrostatic pick-up
b): Equivalent circuit

which is transformed in the output load into:

$$V_{out} = \sqrt{R_o R}\ \omega \frac{\ell}{v_b} \frac{2\Delta x}{d} i_b \qquad (39)$$

for a lossless transformer.

Taking into account the ohmic losses of the coil (Q_o = quality factor of the resonant circuit, Q_L = loaded quality factor), one obtains:

$$S_\Delta = \frac{2}{d}\sqrt{\frac{R_o \omega Q_L}{C}}\frac{\ell}{v_b}\left(1 - \frac{Q_L}{Q_o}\right) \quad . \tag{40}$$

This technique has been used in the CERN SPS, for a dedicated, very sensitive Schottky detector[5] (sensitivity: 75Ω/mm).

2.2 Pick-up evaluation using the reciprocity theorem

The reciprocity theorem, well known in antenna theory, results from Maxwell equations applied to a linear, isotropic system. If we have two sets of current sources in the system J' and J'' which produce the electric fields E' and E'' and the magnetic fields H' and H'', the following relation is valid:

$$\iint_S (E'' \times H' - E' \times H'').\vec{n}ds = \iiint_V (E'.J'' - E''.J')\, dv \tag{41}$$

where the volume v is enclosed by the surface s ($\vec{n}$ is the unity vector on that surface).

For the application of the reciprocity theorem, (Fig. 20), we take $\vec{J'} = \vec{i}_b$, ($\vec{i}_b$ is the beam current along the detector axis), and $J'' = I_1$ (I_1 is a pure current source applied across the load resistor R_o).

We consider an integration volume limited by the metallic enclosure of the pick-up, where the electric fields are normal to the surface, which makes the left side of Eq. (41) vanish and leads to:

$$\iiint_V \vec{E}_b.\vec{I}_1\, dv = \iiint_V \vec{E}''.\vec{i}_b\, dv \tag{42}$$

$$I_1.V_{out} = \int_z E_z.i_b\, dz \tag{43}$$

where V_{out} is the output voltage of the detector when excited by i_b, and E_z is the on axis component of the field in the pick-up structure when excited by I_1. For a given geometry and a given field configuration, E_z can be related to I_1, from power considerations. Then application of Eq. (43) directly gives the detector sensitivity $S=V_{out}/i_b$, for cases where the image current approach would fail (e.g. microwave structures).

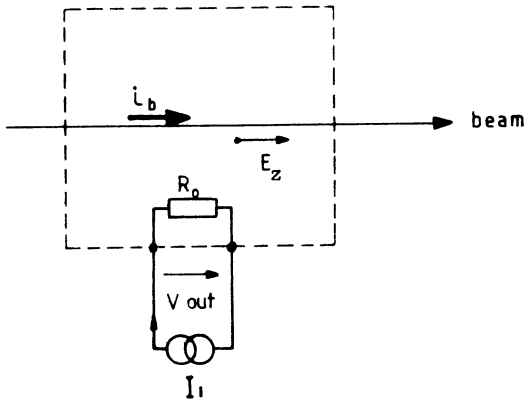

Fig. 20 Application of the reciprocity theorem to a beam detector

Note that the reciprocity theorem , transposed in circuit theory, simply states that, for a passive quadrupole, the determinant of its transfer matrix is unity.

Application of the reciprocity theorem will be illustrated in the following by two examples: the slow-wave and the slot-line pick-ups.

The slow-wave pick-up is essentially an electromagnetic wave guide in which the phase velocity has been slowed down to match the velocity of the particles. Dielectric slabs (Fig. 21a) or corrugations (Fig. 21b) have been considered for this purpose[6]. A description of the field in the structure will be given by standard wave guide theory. With respect to the transverse dimension, the E_z field configuration is either symmetrical (even mode) or antisymmetrical (odd mode), leading to a longitudinal or a transverse detector respectively.

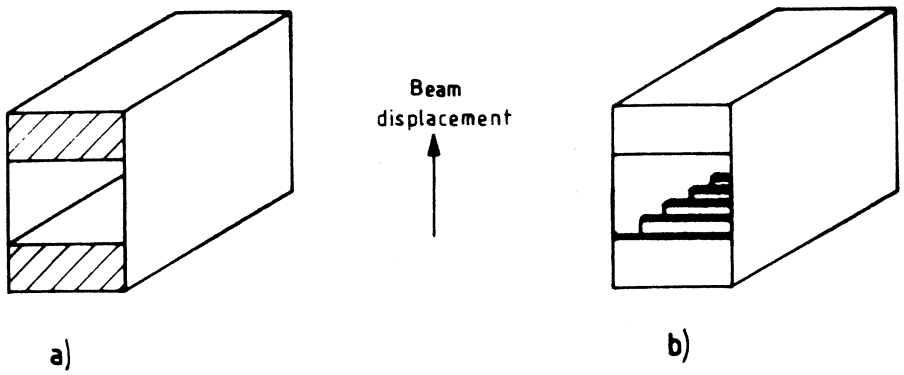

Fig. 21 Slow-wave pick-ups a) dielectric slab
b) corrugated wall

In the case of a pure travelling-wave structure, terminated at both ends by resistors R_o via matched transitions, the power flow P_o in the waveguide is related to I_1 by:

$$P_o = \frac{1}{2} R_o \left(\frac{I_1}{2}\right)^2 \quad . \tag{44}$$

Note that only $I_1/2$ flows towards the waveguide, the rest being dissipated in the load resistor R_o.

The sensitivity is given by:

$$\int_z E_z i_b \exp\left(jk_o z/\beta_p\right) dz = I_1 V_{out} \quad . \tag{45}$$

It is found to be proportional to the transit time factor:

$$\frac{\sin k_o\left(\frac{1}{\beta_p} - \frac{1}{\beta_\varphi}\right)\frac{\ell}{2}}{k_o\left(\frac{1}{\beta_p} - \frac{1}{\beta_\varphi}\right)\frac{\ell}{2}} \tag{46}$$

k_o, β_φ, β_p: propagation constants in free space, waveguide and beam respectively.

The sensitivity is optimum for β_p and β_φ (synchronism condition) as expected. For a given frequency, optimum dimensions of the waveguides are given by the synchronism condition (as in Fig. 14b). Making the detector longer increases the sensitivity (proportional to ℓ) but reduces its bandwidth according to (46).

The slot-line pick-up[7,8] offers another interesting example, in which the waves propagate in a direction perpendicular to that of the beam (Fig. 22). A thin slot in a metallic plane on a dielectric substrate can support quasi TEM waves in the upper region. The electric field, not too close to the slot, is purely tangential: its amplitude is given by:

$$E_\varnothing = V_o \frac{k_c}{2j} H_1^{(1)}(k_c r) \tag{47}$$

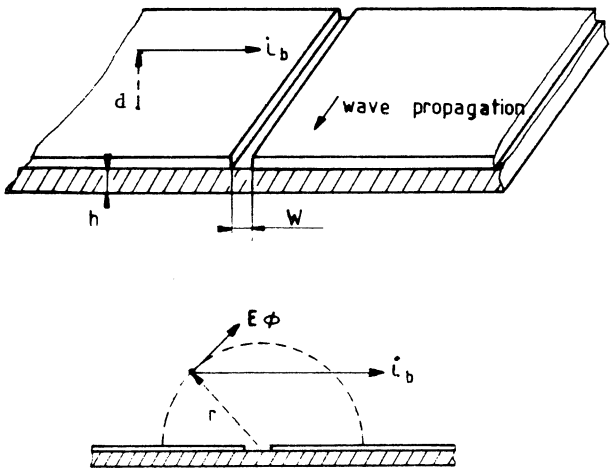

Fig. 22 Schematics of slot-line pick-up

with:

$$k_c = \frac{2\pi j}{\lambda}\sqrt{\left(\frac{\lambda}{\lambda'}\right)^2 - 1} \tag{48}$$

V_o is the voltage across the slot, λ' the wavelength along the slot and $H_1^{(1)}$ the Hankel function of first order.

The longitudinal field E_z, along the beam (at a distance d from the metallic plane) is simply:

$$E_z = \frac{d}{r} E_\phi \quad . \tag{49}$$

For $\lambda' \sim \lambda$ (ε_r not too large) one can replace $k_c H_1^{(1)}(k_c r)$ by $2j\pi r$, which gives:

$$E_s = \frac{V_o}{\pi}\frac{d}{r^2} \tag{50}$$

V_o is related to the power flow P_o along the gap by the slot-line impedance Z: $P_o = V_o^2/2Z$. Combined with (44) and (45), one obtains:

$$S = \frac{\sqrt{R_o Z}}{2}\int_z \frac{1}{\pi}\frac{d}{r^2}\cos\frac{2\pi z}{\lambda}\,dz \tag{51}$$

$$S = \sqrt{\frac{R_o Z}{2}}\exp\left(-\frac{2\pi d}{\lambda}\right) \quad . \tag{52}$$

Equation (52) can be shown to be valid also even if λ and λ' are not very close: λ should then be replaced by λ' in (52).

It is interesting to remark that in the limit $d \ll \lambda$, Eq. (52) reduces to $S = \sqrt{R_o Z/2}$ which is the result given by the image current approach. With the reciprocity theorem, transverse propagation which was previously neglected can be taken into account.

If the signals of two symmetrical plates with two slots are combined, a transverse detector can be built. Its sensitivity would be:

$$S_\Delta = \sqrt{\frac{R_o Z}{h}}\,\frac{1}{\sinh(\pi h/\lambda')} \tag{53}$$

h being the distance between plates.

Slot-line pick-ups would be interesting, because they can be easily produced by standard printed-circuit techniques, even in the microwave region. Their bandwidth is only limited by that of the slot-line to strip-line transitions (the wave on the slot is coupled to outside via a strip line deposited on the opposite side of the dielectric). Because of the transverse propagation, the inherent delay of the detector depends on the transverse beam position. This could be useful for some stochastic cooling schemes.

2.3 Impulse response

Consider again a travelling wave detector like, for instance, the corrugated wall waveguide, where a number of cells (or individual rectangular boxes) are coupled together via the beam pipe. When excited by a short beam pulse, the response of the detector is, in first approximation, an RF burst (Fig. 23) of amplitude V_{out} and duration τ. After the time τ, all the energy deposited in the detector has been transported with the group velocity v_g to the end of the structure and then to the terminating resistor R_o.

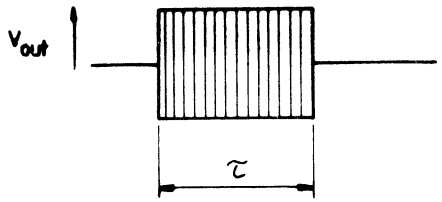

Fig. 23 Impulse response of a travelling-wave detector

What is the relation between the detector sensitivity S and its ouput voltage V_{out} in this case? If we assume a periodic train of short beam pulses (charge q), separated in time by τ, the RF component of the beam current i_b at the central frequency of the pick-up is simply $i_b = 2q/\tau$. Obviously the ouput amplitude V_{out} is constant, with that particular beam input, which gives:

$$V_{out} = S\, i_b = 2Sq/\tau \tag{54}$$

for the longitudinal case and:

$$V_{out} = 2S_\Delta\, q\, \Delta x/\tau \tag{55}$$

for the transverse case.

The energy W deposited by the charge q in the detector is related to the geometry of the structure via its "loss parameter" defined by:

$$W = k\, q^2 \quad . \tag{56}$$

The k factor is also the R/Q of the structure ($k = \frac{1}{2}\, \omega_o\, R/Q$).

Combining (54), (56) and the relation:

$$W = \frac{1}{2} \frac{V_{out}^2}{R_o} \tau \tag{57}$$

valid for a lossless detector one finds:

$$S = \sqrt{\frac{R_o k \tau}{2}} \tag{58}$$

and a similar equation for the transverse case.

The loss parameter k depends essentially upon the cell geometry, and can be calculated analytically in some simple cases (neglecting the effect of the beam hole) or evaluated by computer codes like SUPERFISH for instance. On the other hand τ characterizes the cell-to-cell coupling via v_g.

From Eq. (58), the maximum sensitivity is again proportional to ℓ (detector length) as both k and τ are themselves proportional to ℓ. Of course the bandwidth decreases correspondingly as was shown in the example of the multiple directional coupler (Fig. 14b). Note that this multiple directional coupler can be considered as a backward-travelling wave structure with $v_g = c$.

In the following example, we shall evaluate the k factor for the simple geometry of Fig. 24: a chain of coupled cylindrical cavities. We consider the mode E_{o11} (transverse detector) where the electric field is only longitudinal:

$$E_x = E_\phi = 0; \quad E_z = E_o J_1(2\pi x/\lambda) \cos \phi \tag{59}$$

The energy lost by charge q is given by:

$$W = \frac{1}{2} q \int_\ell E_z \exp j\frac{\omega z}{c} \, dz \quad . \tag{60}$$

The factor 1/2 simply reflects the fact that the charge q only sees one half of its own induced voltage (fundamental theorem of beam loading). W is also obtained by integrating E_z^2 over the whole cavity volume:

$$W = \frac{1}{2} \iiint \varepsilon_o E_z^2 \, dv \quad . \tag{61}$$

Eliminating E_o between (59), (60) and (61) finally gives:

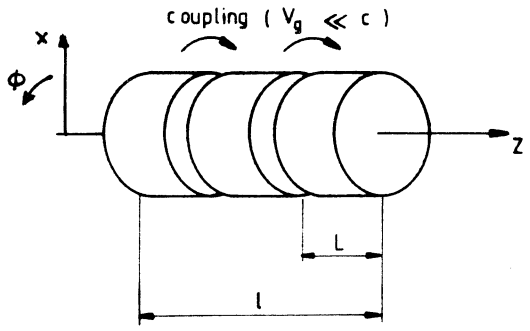

Fig. 24 A chain of coupled cylindrical cavities as transverse detector

$$W = \frac{\mu_o}{4\pi} \frac{\ell\omega^2}{2.38}\left(\frac{2\pi}{\lambda}\right)^2 \left(\frac{\sin(\pi L/\lambda)}{\pi L/\lambda}\right)^2 q^2 x^2 \quad . \tag{62}$$

Equation (62) shows the interest of high-frequency detectors as far as sensitivity is concerned (factors ω^2 and $1/\lambda^2$). But the influence of the beam hole which has been neglected in this simplified analysis will become more and more important. An example of this type of detector, using the first transverse mode of the accelerating cavities in the CERN SPS is given in Ref. 9.

3 OBSERVATION OF SCHOTTKY SIGNALS

3.1 Spectral analysis

As already mentioned in section 1 the measurement of the power spectral density of the Schottky signals gives the particle distribution in either momentum or betatron tune (or a combination of both). Therefore, spectral analysis is the natural technique for observing Schottky signals.

The frequency span of interest is of the order of the revolution frequency, or even less, (in most cases below 100 kHz). Consequently, the Fast Fourier Transform (FFT) or, more precisely, the Digital Fourier Transform (DFT) techniques which operate at low frequencies, can be used to evaluate in real time the signal spectrum. The Schottky band to be analysed must be translated at low frequency prior to FFT analysis, as in a conventional spectrum analyser. This may require a careful prefiltering to reject the unwanted image frequencies.

In the DFT technique, the signal is sampled and digitized at frequency f_s. Each digital word is stored in a memory with M locations (typically 2^{10} = 1024 locations): the duration of the signal sample to be analysed is then $T = M/f_s$. The frequency content (frequency span) of the sampled signal extends only up to $f_s/2$ (Nyquist theorem), and the resolution of the frequency analysis is of the order of 1/T (Fig. 25).

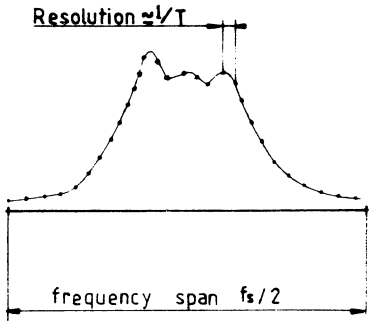

Fig. 25 Spectral analysis (DFT) of Schottky signals

Depending on the choice of the signal processing "windowing", the resolution varies a little: 1/T for the rectangular window; 1.4/T for the "Hamming window", better optimized for noise signals.

For a given resolution of the beam distribution measurement (in $\Delta p/p$, or $\Delta Q/Q$), T is minimum for the largest width of the Schottky band. For instance, in the longitudinal, debunched beam case, one would minimize T by looking at the highest frequency Schottky bands (width $n\Delta f$) limited by either $f_s/2$, the detector sensitivity, or the overlap condition. This is of particular interest for the observation of "pseudo" Schottky signals in pulsed machines to measure the beam momentum spread during debunching. (T is there strictly limited by the duration of the magnetic cycle flat top). The beam develops, during debunching at high intensity, a very complicated structure which is more or less equivalent to random noise, but of macroscopic nature ("pseudo" Schottky signal). Its spectrum analysis provides an estimate of the momentum spread of the beam during debunching.

Even if T can be made very long, the result of the DFT on a noise signal does not give a good estimate of its spectral density. This is because the variance of the power measurement is comparable to its mean value: it does not decrease when T is made longer.

A better "estimation" of the true power density is obtained by averaging several spectra taken at different time intervals. The "degree of confidence" of the measurement increases with the number of averaged spectra (Fig. 26), at the expense of the total analysis time (which may be distributed over several machine cycles in the the previous example).

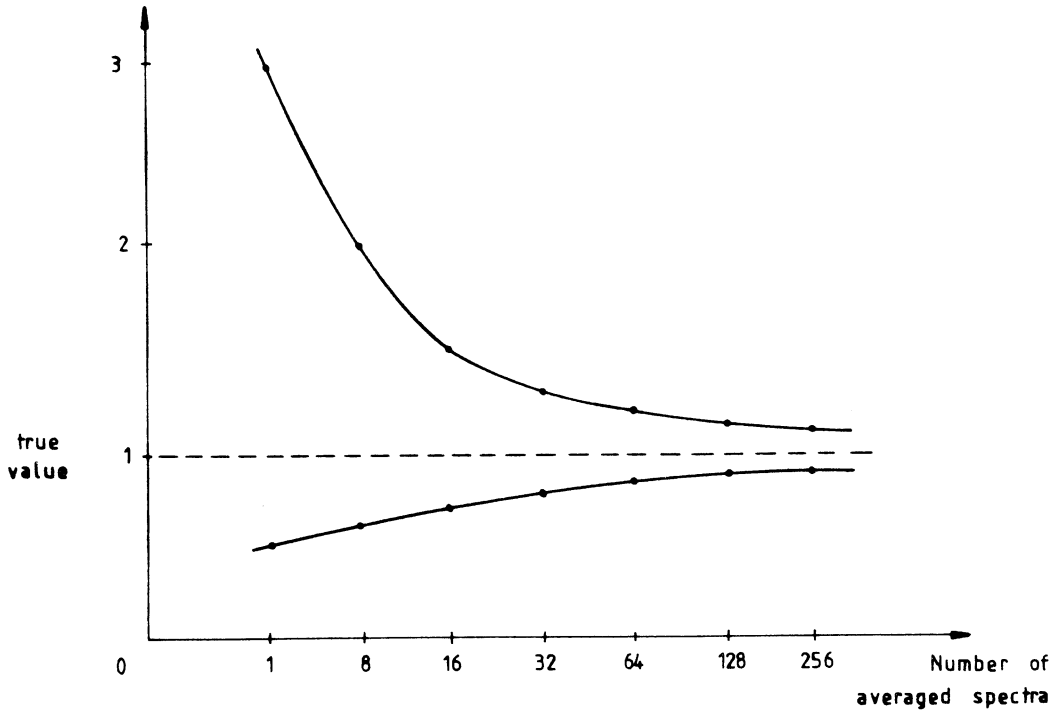

Fig. 26 90% confidence level of the noise spectral density measurement

3.2 Parasitic signals of the Schottky spectrum

Due to the very low level of the Schottky signals, many sources of disturbance can be harmful and should be eliminated whenever possible.

Parasitic signals may come from the beam itself; if there is a coherent excitation (i.e. transverse) it will appear as a betatron signal, but with an amplitude proportional to N and not $\sqrt{N}$ as for the Schottky signal. The longitudinal line in a transverse Schottky scan can be suppressed by careful centering of the pick-up on the beam axis. In the bunched beam case, additional sharp filtering with a crystal filter is necessary[5].

The line related components are reduced by a careful design of the amplifiers, power supplies and earth connections. If this is not sufficient, narrow band synchronous filtering (locked to the mains frequency) can also be employed.

Of more fundamental nature is the disturbance due to the thermal noise of the first preamplifier, after the detector. The amplifier is characterised by its noise factor F (excess noise with respect to a simple resistor R_o). The available noise spectral density resulting from the amplifier and which is given by: $Fk_o t_o R_o$, (k_o: Boltzmann constant, t_o: temperature) must be considerably smaller than the Schottky noise spectral density. One possibility is to cool the preamplifier and the terminating resistors of the

pick-ups (ACOL). From Fig. 2, it is clear that the best signal to noise ratio is obtained at low frequencies (for the case of unbunched beams). Unfortunately, observation of Schottky signals at high frequency is more favourable as far as sensitivity and analysis time are concerned.

3.3 Bunched-beams signal processing

As all Schottky lines in a frequency interval f_b are correlated (see section 1), it is interesting to sample the beam signal at the revolution frequency. All lines will be folded in the base band giving a much better signal to noise ratio as will be shown in the following.

Consider the RF burst amplitude V_{out} of Fig. 23 delivered by a travelling wave transverse pick-up, when excited by a short bunch. For a transverse r.m.s. beam displacement x, the output voltage of the detector and the thermal noise voltage of the amplifier, referred to the input, are respectively:

$$V_{rms} = 2S_\Delta q\, x/\tau \tag{63}$$

$$V_{th} = \sqrt{F k_o t_o R_o B} \tag{64}$$

B being the amplifier bandwidth.

The power signal to noise ratio, during the time interval τ is therefore:

$$\frac{1}{U} = \frac{2\, N\, e^2 S_\Delta{}^2\, x^2}{F\, \tau^2\, k_o\, t_o\, R_o\, B} \tag{65}$$

This is also the signal to noise ratio after sampling. We can select B ($B = B_{opt}$) to optimize 1/U. B_{opt} is the minimum bandwidth for which the useful signal is not reduced significantly. This happens if the rise time of the band limited RF burst is of the order of its length: $1/B \simeq \tau$, as illustrated in Fig. 27. More precisely B_{opt} is that of the so called "optimum filter" (radar terminology) for which the impulse response is the time reversed image of the RF burst. With that condition (65) becomes:

$$\frac{1}{U} = \frac{1}{\tau f_o}\, N\, \frac{e^2\, f_o\, S_\Delta{}^2\, x^2}{F\, k_o\, t_o\, R_o} \tag{66}$$

which is the same as for the debunched beam case, except for the enhancement factor $1/\tau f_o$ which can be much larger than unity[10].

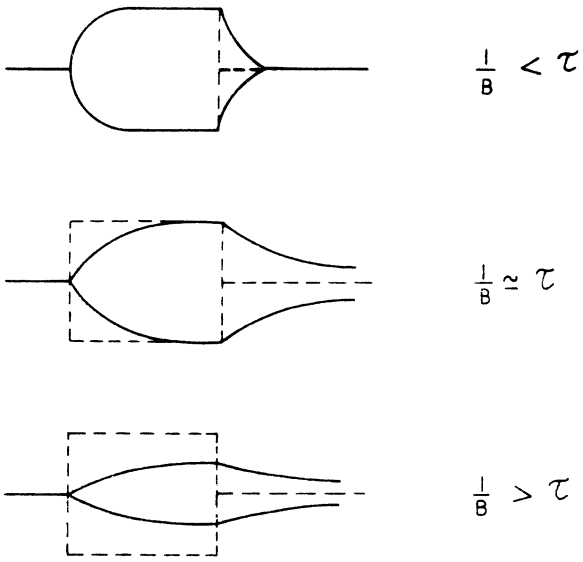

Fig. 27 Optimum filtering of an RF burst from a beam detector

The overall signal processing system for a bunched beam transverse Schottky signal is displayed on Fig. 28. Frequency translation down to the base band frequency can be done by peak detection, as indicated, or with a synchronous detector driven by the sum signal of the pick-up. In this case, it is interesting to remark that the odd synchrotron satellites are rejected for an in phase detection (like for a peak detection), whereas for a quadrature detection, it is the even synchrotron satellites which are rejected. This feature may be useful if one wants to isolate the central J_o line of the Schottky band.

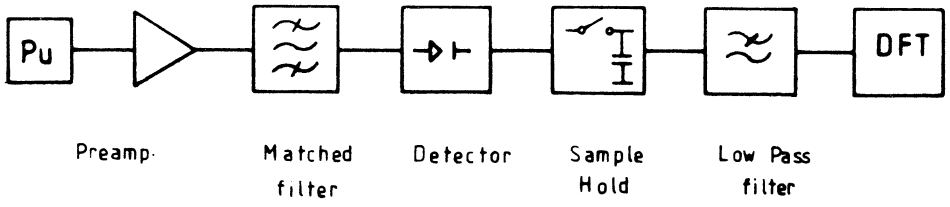

Fig. 28 Bunched beam signal processing system

Although the thermal noise of the preamplifier is of less importance for bunched beam signal processing, the effect of spurious coherent excitation of the beam may be more of a problem. This is because, even a low frequency excitation, near the first betatron line, appears everywhere in the spectrum, contrary to the debunched beam case, and may spoil even a high frequency Schottky system. A solution to that problem is to reject that part of the detector signal which is coherent from one bunch to the next[9].

4 BEAM TRANSFER FUNCTIONS

4.1 Principle of beam transfer functions

The name of beam transfer function almost speaks for itself: it relates the response of the beam (amplitude and phase) to a known excitation. In the case of a transverse excitation by a deflector (or kicker), the beam response is measured by a transverse pick-up as indicated on Fig. 29a, whereas Fig. 29b shows the arrangement for the measurement of a longitudinal transfer function[11].

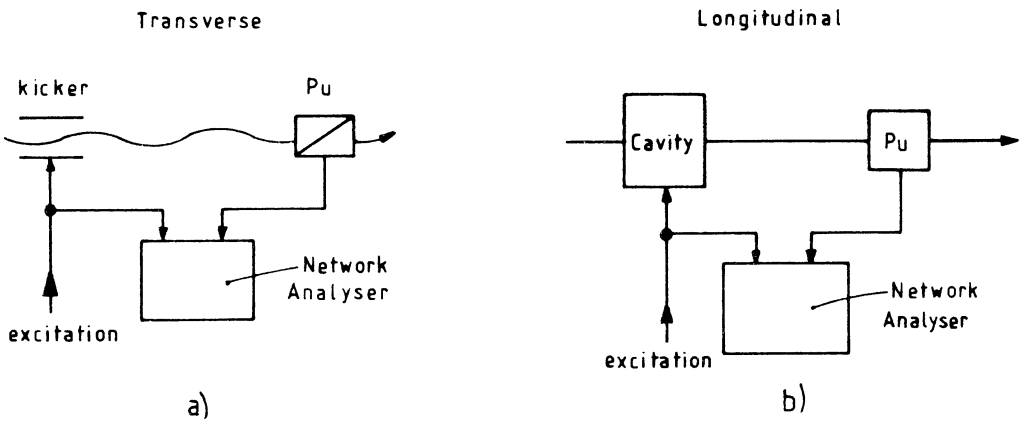

Fig. 29 Principle of beam transfer function measurement

To minimize the analysis time and the disturbance to the beam, it is interesting to excite the beam with a white noise spectrum (all frequencies are present in the band of interest). There the output will also be a noise signal, similar to the Schottky noise, and for which similar processing techniques can be applied. To extract the phase information spectral density measurements are not sufficient and a dual channel DFT instrument is needed. Again averaging many transfer functions reduces the variance of the estimate (Fig. 26). In Fig. 29a and b, a new element appears, namely the kicker (either transverse or longitudinal) which will be examined more in detail in the following.

4.2 Kickers

A longitudinal kicker is a fairly straightforward device in which a longitudinal electric field E_z is produced. The particle gains an energy ΔW, when crossing the kicker (or cavity), which is simply given by:

$$\Delta W = \int_z e\, E_z\, dz \quad . \tag{67}$$

The application of the reciprocity theorem to a longitudinal beam detector has led us to Eq. (43), which combined with (67) results in:

$$\Delta W = e\, S\, I_1 \tag{68}$$

showing that the energy gain of the kicker and the sensitivity of the pick-up are simply proportional. In other words a longitudinal kicker is nothing but a longitudinal detector working in reverse. This is almost obvious for cavity like detectors, but is also true for a directional coupler type of pick-up for instance, where a quasi TEM wave propagates. There, only the field at the ends of the coupler are useful for beam excitation.

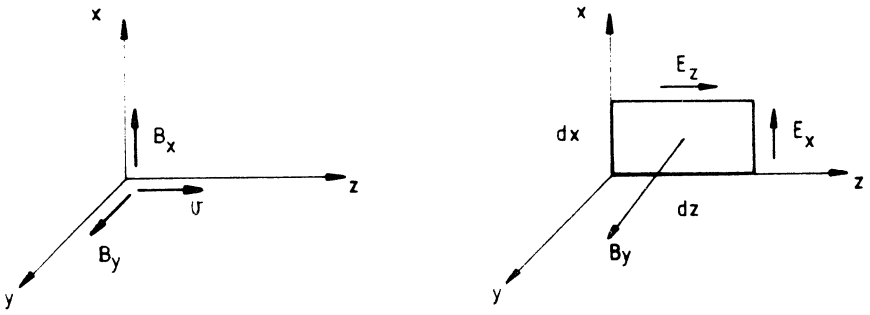

Fig. 30 Application of the induction law to the evaluation of the transverse force

Consider now the case of a transverse deflection produced by the Lorentz force:

$$\vec{\Delta p} = \int_z e\,(\vec{E} + \vec{v} \times \vec{B})\,dz \tag{69}$$

which projected on the x axis (Fig. 30) can be written:

$$\Delta p_x = \int_z e\,(E_x + v.B_y)\,dz \quad . \tag{70}$$

To evaluate the quantity $E_x + v.B_y$, we apply the induction law to a small rectangle in the x0z plane:

$$\oint_C \vec{E}.d\vec{\ell} = -\frac{\partial}{\partial t}\,\phi_B \tag{71}$$

ϕ_B being the flux of the magnetic field B on the contour C. One obtains

$$\frac{dE_z}{dx}\,dx\,dz + \frac{dE_x}{dz}\,dz\,dx = -j\omega\,B_y\,dx\,dz \tag{72}$$

$$\frac{dE_z}{dx} + \frac{dE_x}{dz} = -j\omega\,B_y \tag{73}$$

With:

$$\frac{dE_x}{dz} = \frac{dE_x}{dt}\frac{dt}{dz} = j\omega E_x \frac{1}{v} \tag{74}$$

it comes:

$$E_x + v.\ B_y = \frac{v}{j\omega}\frac{dE_z}{dx} \tag{75}$$

Equation (75) shows that only the longitudinal field E_z (more precisely dE_z/dx) is important for transverse deflection. This is a well known result (linac theory for instance) which has a few interesting corollaries. For instance, one cannot deflect a beam neither with a pure TEM wave nor with a pure H mode in a cavity if the end effects are neglected. A transverse kicker must show a longitudinal electric field, in the same way as a transverse pick-up extracts energy from the longitudinal velocity of the particles. There is complete equivalence between pick-ups and kickers even in the transverse plane. This will be illustrated in the following example.

The "TEM" travelling wave kicker has the same geometry as the transverse directional coupler pick-up (Fig. 31a). The field is that of a TEM wave along the two lines, except at the two ends where a longitudinal component E_z exists (Fig. 31b). Assume, for simplicity $v_p = v_\varphi$: the particles receive successively two opposite transverse kicks at either end of the kicker, the result being a zero deflection (another way of saying the same thing is that the electric and magnetic deflections along the line exactly cancel each other). On the contrary, for $v_p = -v_\varphi$ (beam in the opposite direction) the two kicks add exactly if they are separated by half a period of the RF wave ($\ell = \lambda/4$). This gives a variation of the type $\sin 2\pi\, \ell/\lambda$. The kicker efficiency $K_\perp$ is, from Eq. (75) proportional to:

$$K_\perp \sim e\frac{v}{j\omega}\frac{dE_z}{d_x} \sin 2\pi\, \ell/\lambda \tag{76}$$

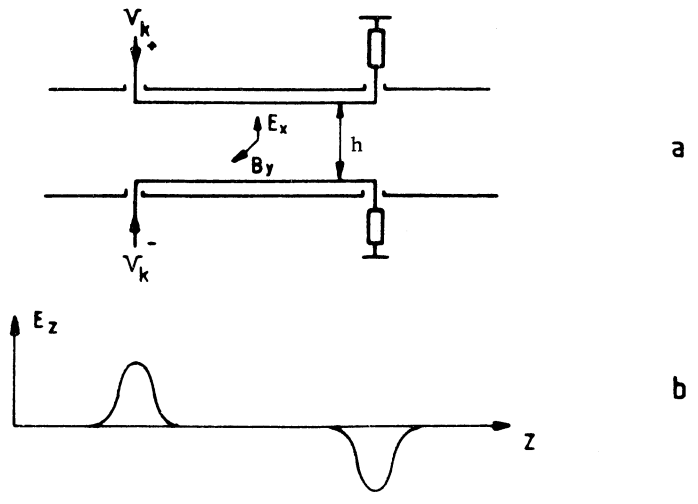

Fig. 31 "TEM" travelling wave kicker

which can be written:

$$K_{\perp} \sim \frac{e}{h}\, \ell \quad \frac{\sin\frac{2\pi\ell}{\lambda}}{\frac{2\pi\ell}{\lambda}} \tag{77}$$

for $v = c$.

The first term is proportional to the DC deflection (proportional to ℓ) and the term in brackets gives the form factor which is frequency dependent.

4.3 Debunched beam transfer function

The beam is composed of a collection of particles, each having its own oscillation frequency $q_i\omega_i$, submitted to a common driving force $F(\omega)$. The equation of motion, for each individual particle is, in linear approximation:

$$\ddot{x}_i + (q_i\omega_i)^2\, x = F(\omega) \tag{78}$$

with a forced solution of the form:

$$\begin{aligned} x_i &= X_i \exp j\omega t \\ X_i &= \frac{F(\omega)}{(q_i\omega_i)^2-\omega^2} \simeq \frac{1}{2\omega}\,\frac{F(\omega)}{\omega_i q_i-\omega} \end{aligned} \tag{79}$$

The average beam response $\langle X_i\rangle/F(\omega)$ is given by the integral:

$$\frac{\langle X_i\rangle}{F(\omega)} = \frac{1}{2\omega}\int_{q_1\omega_1}^{q_2\omega_2} \frac{\rho(q_i\omega_i)}{q_i\omega_i-\omega}\, d(q_i\omega_i) \tag{80}$$

where $\rho(q_i\omega_i)$ is the normalized distribution of the betatron frequencies within the beam, ($q_1\omega_1$ and $q_2\omega_2$ being the two extreme frequencies).

This is a singular integral because of the pole at $q_i\omega_i = \omega$. It can be decomposed into its Cauchy principal value, which is real, and its residue at the pole (imaginary):

$$\frac{\langle X_i\rangle}{F(\omega)} = \frac{1}{2\omega}\,[\text{Princ. Value} - j\pi\rho(\omega)] \tag{81}$$

We now replace $\langle X_i\rangle$ by $j\omega\langle X_i\rangle$ to obtain a real transfer function $B(\omega)$ when energy is absorbed (force and displacement in quadrature) and obtain:

$$B(\omega) = \frac{1}{2}\,(\pi\rho(\omega) + j\ \text{Princ. Value}) \quad . \tag{82}$$

The real part of the transfer function gives the particle distribution in tune like the spectral power density of the Schottky signal. Outside the frequency band $(q_1\omega_1, q_2\omega_2)$ the real part of $B(\omega)$ vanishes (pure imaginary response). The fact that a collection of lossless oscillators responds like a damped resonator is the basis of Landau damping and is illustrated in Fig. 32.

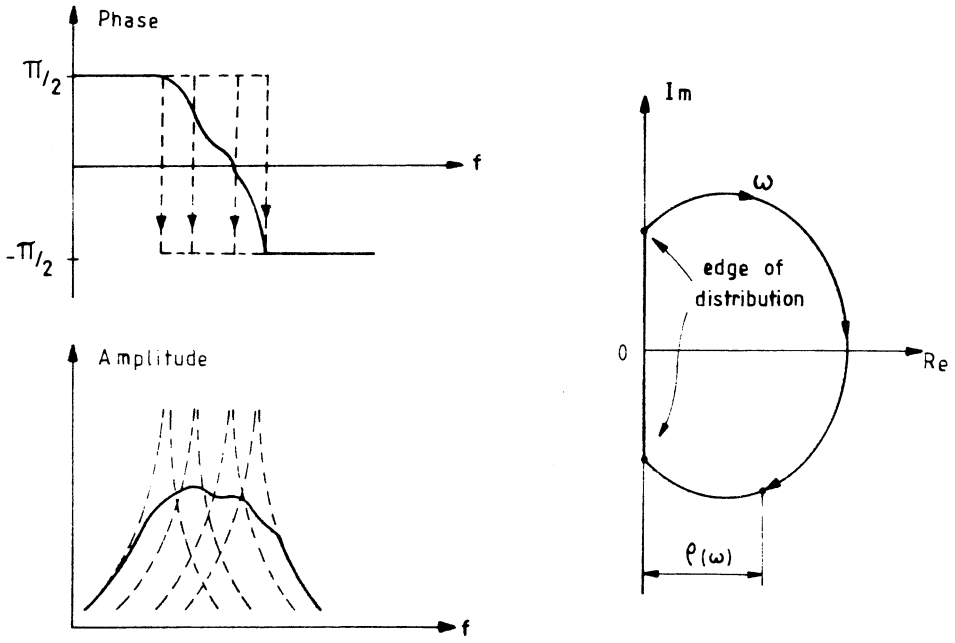

Fig. 32 Response of a large number of lossless resonators
- - - individual particles
_____ average

The evaluation of the stability of the beam certainly corresponds to the most interesting application of beam transfer function measurements. Collective effects (and in particular beam instabilities) result from the presence of parasitic impedances in the machine which generate a deflecting force (in the transverse case), when excited by a collective displacement of the beam. In other words the excitation $F(\omega)$ in Eq. (78) should be combined with a term proportional to the beam response $j\omega\langle X_i\rangle$. This leads to the well known feedback loop of Fig. 33, where $H(j\omega)$ is linked to machine parameters and is proportional to the impedance of the machine $Z(\omega)$. For instance in the transverse case:

$$H(j\omega) = j\frac{e\omega_o i_b}{2\pi m_o c\gamma}\, Z(\omega) \tag{83}$$

m_o is the rest mass of the particle.

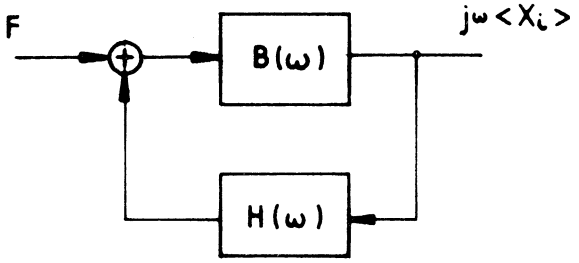

Fig. 33 Feedback loop due to the machine impedance

From Fig. 33 the new transfer function becomes:

$$B'(\omega) = \frac{j\omega\langle X_i\rangle}{F} = \frac{B(\omega)}{1-B(\omega)H(\omega)} \tag{84}$$

$$\frac{1}{B'(\omega)} = \frac{1}{B(\omega)} - H(\omega) \quad . \tag{85}$$

By plotting the curve $1/B(\omega)$ for different beam intensities i_b one obtains a family of curves shifted in the complex plane by the quantity $H(\omega)$ (Fig. 34). This shift being proportional to $Z(\omega)$, the machine impedance can be directly measured at any frequency[11].

When the shifted $1/B(\omega)$ curve reaches the complex plane origin, stability of the beam is lost ($B(\omega) \to \infty$), this means that the distance of the curve to the origin is a measure of beam stability. If a feedback system is employed to stabilize the beam, its effect which should be to shift the curve towards the right side of the complex plane could also be evaluated.

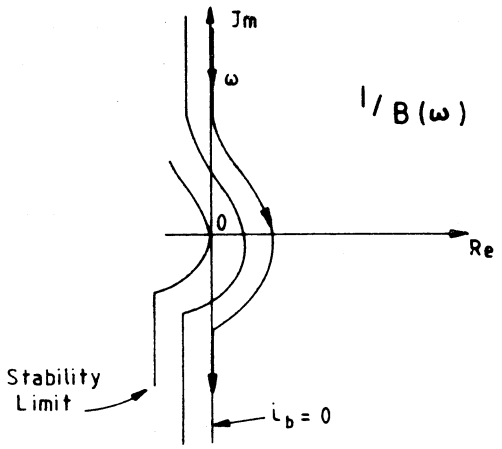

Fig. 34 Evaluation of the beam stability with transfer function measurements

With very sensitive detectors and provided long analysis times are available (DC storage rings), beam transfer function is a very powerful technique, almost non-disturbing to the beam; it can also be used in a similar way for the longitudinal plane.

4.4 Bunched-beam transfer function

The main difference with respect to the unbunched beam case is that an excitation of the beam at a given frequency ω, not only results in a beam response at ω, but also at all frequencies $n\omega_o \pm \omega$. (This is because the bunched beam samples the ω waveform at the revolution frequency ω_o). The process is therefore fundamentally nonlinear, and as a consequence, the beam transfer function is not defined in general, unless additional conditions are imposed[12]. For instance, if bunch to bunch coupling can be neglected, one can define unambiguously the beam transfer function of a single bunch, for a given mode of oscillation (dipole, quadrupole etc.), i.e. within an f_b frequency interval. Another interesting case is when the bunched beam behaves like an unbunched beam: many equal bunches, frequency range from DC up to $f_{RF}/2$ and negligible effects beyond.

In the transverse plane, the measurement of the machine tune is nothing but a beam transfer function measurement. Many descriptions of tune measurement systems exist in the literature; excitation can be sinusoidal or random (band limited noise) near a betatron line, or pulsed; beam measurement could be at the same or at different frequency. In general the machine impedance $Z(\omega)$ cannot be measured directly, as a function of frequency; on the other hand if the shape of $Z(\omega)$ is known (e.g. resistive wall) one can determine its magnitude by measuring the tune shift as a function of beam intensity.

The RF system and its associated feedback loops strongly perturbs the longitudinal transfer function of a bunched beam. This is particularly true for the dipole mode; fortunately the quadrupole mode is easier to analyse and can provide meaningful measurements of the machine impedance. Amplitude modulation of the RF waveform at around twice the synchrotron frequency excites the quadrupole mode of a single bunch; the quadrupole oscillation can be observed in a very simple way by peak detecting the bunch signal from a wide band longitudinal detector.

The measured beam transfer function, at low intensity shows a sharp phase discontinuity, at the bunch center, where the particle density is maximum, and a smooth phase curve near the bunch edge (Fig. 35a). This corresponds to the $1/B(\omega)$ plot in Fig.35b and provides a direct measurement of the center synchrotron frequency. At higher intensities, the inductive wall effect shifts the $1/B(\omega)$ curve along the imaginary axis (real frequency shift) and the phase curve of Fig. 35a shows a sharper transition. From those measurements, the magnitude of $Z(\omega)/n$ for the inductive wall case can be determined over a frequency interval of the order of f_b.

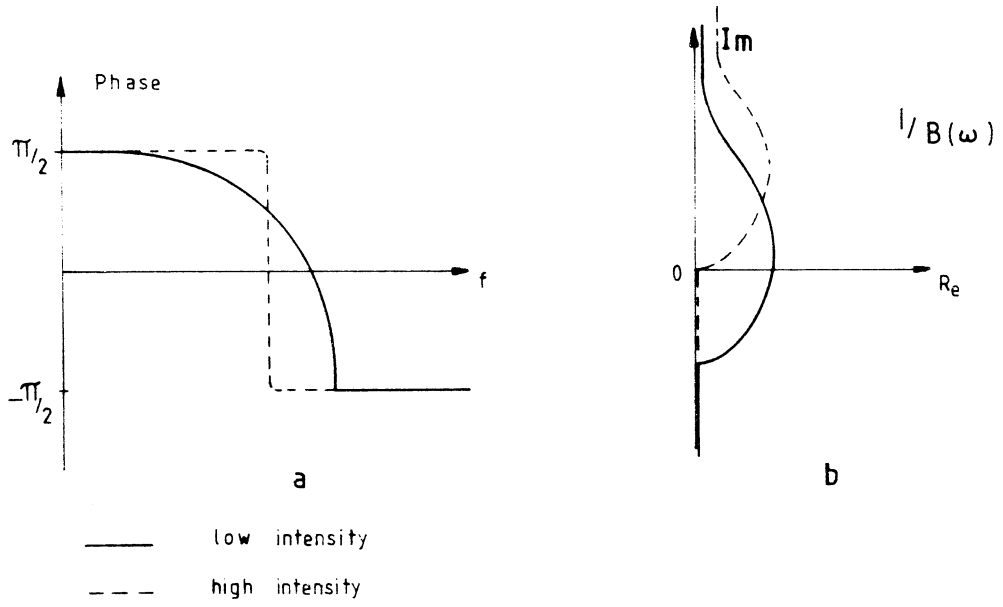

Fig. 35 Quadrupole-mode transfer function (bunched beam)

* * *

REFERENCES

1) J. Borer, P. Bramham, H.G. Hereward, K. Hübner, W. Schnell, L. Thorndahl, Non-destructive diagnostics of coasting beams with Schottky noise. IXth Int. Conf. on High Energy Accelerators, SLAC, May 1974, (SLAC, Stanford, 1974).

2) H.G. Hereward, W. Schnell, Statistical phenomena, Proc. of the first course of the Int. School of particle accelerators, Erice, Sicily, 1976 (CERN 77-13, 1977).

3) T. Linnecar. The high frequency longitudinal and transverse pick-ups used in the SPS. CERN SPS/ARF/78-17, (1978).

4) J. Borer, R. Jung, CERN Accelerator School, Antiprotons for colliding beam facilities, CERN, 1983, (CERN 84-15, 1984).

5) T. Linnecar, W. Scandale. A Transverse Schottky noise detector for bunched proton beams. IEEE Trans. Nucl. Sci., NS-28 page 2147 (1981).

6) D. Boussard, G. Di Massa, High frequency slow wave pick-ups, CERN SPS/86-4, (1986).

7) F. Caspers, Planar slotline pick-ups and kickers, CERN PS/AA Note 85-46, (1985).

8) D. Boussard, Evaluation of slot line pick-up sensitivity, CERN SPS/ARF Note 85-9 (1985).

9) D. Boussard, T. Linnecar, W. Scandale, Recent developments on Schottky beam diagnostics at the CERN SPS collider, IEEE Trans. Nucl. Sci. NS-32 page 1908 (1985).

10) D. Boussard, S. Chattopadhyay, G. Dôme, T. Linnecar, Feasability study of stochastic cooling of bunches in the SPS, CERN Accelerator School, Antiprotons for colliding beam facilities, CERN, 1983, (CERN 84-15 1984).

11) J. Borer et al., Information from beam responses to longitudinal and transverse excitation, IEEE Trans. Nucl. Sci. NS-26 page 3405 (1979).

12) S. Chattopadhyay, Some fundamental aspects of fluctuations and coherence in charged particle beams in storage rings, CERN 84-11 (1984).